

# On the Energy-Based Variational Model for Vector Magnetic Hysteresis

Leonid Prigozhin<sup>1</sup>, Vladimir Sokolovsky<sup>2</sup>, John W. Barrett<sup>3</sup>, and Sergey E. Zirka<sup>4</sup>

<sup>1</sup>Jacob Blaustein Institutes for Desert Research, Ben-Gurion University of the Negev, Sede Boqer Campus 84990, Israel

<sup>2</sup>Physics Department, Ben-Gurion University of the Negev, Beer-Sheva 84105, Israel

<sup>3</sup>Department of Mathematics, Imperial College London, London, SW7 2AZ, U.K.

<sup>4</sup>Department of Physics and Technology, Dnipropetrovsk National University, 49050 Dnipropetrovsk, Ukraine

We consider the quasi-static magnetic hysteresis model based on a dry-friction-like representation of magnetization. The model has a consistent energy interpretation, is intrinsically vectorial, and ensures a direct calculation of the stored and dissipated energies at any moment in time, and hence not only on the completion of a closed hysteresis loop. We discuss the variational formulation of this model and derive an efficient numerical scheme, avoiding the usually employed approximation, which can be inaccurate in the vectorial case. The parameters of this model for a nonoriented steel are identified using a set of first-order reversal curves. Finally, the model is incorporated as a local constitutive relation into a 2-D finite-element simulation accounting for both the magnetic hysteresis and the eddy current.

**Index Terms**—Energy-based model, finite-element simulation, variational formulation, vector magnetic hysteresis.

## I. INTRODUCTION

THE hysteretic constitutive relation between the magnetization and the magnetic field in ferromagnets remains one of the main difficulties in electromagnetic modeling. The Preisach model [1], providing for, probably, the most accurate macroscopic description for ferromagnetic hysteresis at present, is a black-box-type method for storing, and using for interpolation, a vast amount of experimental data necessary for the implementation of this model. A simpler and very popular Jiles–Atherton model [2] needs a patch to avoid a nonphysical behavior [3], [4]; the physical arguments used for the derivation of this model have been criticized in [5]. Both the Preisach and Jiles–Atherton models are scalar and, although there exist numerous vector modifications, these also lack a true physical justification. Furthermore, in a general situation, the use of these models to predict the evolving magnetization does not make computing the accompanying energy loss straightforward [6].

In a seminal work, Bergqvist [7] proposed a new quasi-static magnetic hysteresis model, phenomenological but having a consistent and genuine energy interpretation, intrinsically vectorial, and ensuring a direct calculation of the stored magnetic energy and the dissipated energy at any moment in time, and not only after the completion of a closed hysteresis loop as is usually the case. This model differs significantly from the previous ones but, like the Jiles–Atherton model, regards the pinning of domain walls as the cause of hysteresis, and presents, similar to the Preisach model, the complex hysteretic behavior as a superposition of reactions of simple hysteretic elements, “pseudoparticles.” Later, the Bergqvist model [7] and models, closely related to it, have been

Manuscript received March 31, 2016; revised May 23, 2016 and June 29, 2016; accepted August 5, 2016. Date of publication August 10, 2016; date of current version November 16, 2016. Corresponding author: L. Prigozhin (e-mail: leonid@math.bgu.ac.il).

Color versions of one or more of the figures in this paper are available online at <http://ieeexplore.ieee.org>.

Digital Object Identifier 10.1109/TMAG.2016.2599143

considered in a series of works (see [8]–[15] and the references therein).

To make the magnetization update at each time step explicit, Bergqvist [7] employed an approximation, turning his vectorial energy-based model into a vector play hysteron model. Such an approximation was used also in almost all the following works: the only exception that we know is [13], where an optimization problem is solved to find the new value of magnetization. Although in the scalar case this approximation does not introduce any error at all, in the general vectorial case it leads to an error that does not disappear as the time steps (external field increments) tend to zero.

In this paper, we avoid such an approximation and propose a more efficient numerical method than in [13]. We start with the derivation and a discussion of a simplified variational hysteresis model in order to clarify its mathematical structure, and then make the model more realistic. We identify the parameters of this model for nonoriented electrical steel using a set of experimental first-order reversal curves (FORCs). Finally, we implement the model as a constitutive relation in a finite-element simulation considering both the quasi-static hysteretic magnetization and the eddy current.

## II. ENERGY BALANCE AND DRY-FRICTION-LIKE MODEL OF MAGNETIZATION

The magnetostatic field energy in a magnetic material can be presented as a sum of the empty space energy, depending on the magnetic field  $\mathbf{h}$ , and the internal energy determined by the material magnetization  $\mathbf{m}$ . The energy density

$$W = \frac{1}{2} \mu_0 h^2 + U(\mathbf{m}) \quad (1)$$

changes as

$$\dot{W} = \mathbf{h} \cdot \dot{\mathbf{b}} - |\mathbf{r} \dot{\mathbf{m}}| \quad (2)$$

where  $\mathbf{b} = \mu_0(\mathbf{h} + \mathbf{m})$  is the magnetic induction,  $\mu_0$  is the permeability of vacuum,  $\mathbf{h} \cdot \dot{\mathbf{b}}$  is the rate of the magnetic

field work, and  $|r\dot{\mathbf{m}}|$  is the rate of dissipation caused by the irreversible movement of the domain walls accompanying the changes in magnetization [7]. For an isotropic material, the “friction coefficient”  $r$  is a positive scalar; otherwise, it is a symmetric positive-definite matrix. Here and below the time derivative of  $\mathbf{u}$  is denoted as  $\dot{\mathbf{u}}$ , and if  $\mathbf{u}$  is a vector,  $u$  means  $|\mathbf{u}|$ . Equations (1) and (2) yield  $\mu_0 \mathbf{h} \cdot \dot{\mathbf{h}} + \nabla U(\mathbf{m}) \cdot \dot{\mathbf{m}} = \mu_0 \mathbf{h} \cdot (\dot{\mathbf{h}} + \dot{\mathbf{m}}) - |r\dot{\mathbf{m}}|$  or

$$(\mathbf{h} - \mathbf{f}(\mathbf{m})) \cdot \dot{\mathbf{m}} = |k\dot{\mathbf{m}}| \quad (3)$$

where  $\mathbf{f}(\mathbf{m}) = (1/\mu_0) \nabla U(\mathbf{m})$  and  $k = (1/\mu_0)r$ .

Unlike the Jiles–Atherton model, where the magnetization  $\mathbf{m}$  is assumed to be a sum of its reversible and irreversible parts, the Bergqvist model of hysteresis uses a similar representation for the magnetic field; this difference is crucial. The field  $\mathbf{h}_r = \mathbf{f}(\mathbf{m})$  is called reversible, because the magnetic work it delivers is fully converted into internal energy; the remaining field  $\mathbf{h}_i = \mathbf{h} - \mathbf{h}_r$  is called irreversible. Equation (3) then takes the form

$$\mathbf{h}_i \cdot \dot{\mathbf{m}} = |k\dot{\mathbf{m}}|. \quad (4)$$

For an isotropic material, (4) is satisfied if the following “dry-friction” constitutive relation is postulated:

$$\begin{aligned} |\mathbf{h}_i| &\leq k; \\ \text{if } |\mathbf{h}_i| < k \text{ then } \dot{\mathbf{m}} &= \mathbf{0}; \\ \text{if } \dot{\mathbf{m}} \neq \mathbf{0} \text{ it has the direction of } \mathbf{h}_i. \end{aligned} \quad (5)$$

We note that this multivalued relation is similar to the relation between the rate of plastic deformation and the stress in an elastoplastic material with the yield strength  $k$ .

To obtain a more convenient formulation of (5), we note that  $\mathbf{h}_i \in \tilde{K} := \{\mathbf{u} \in \mathbb{R}^3 : |\mathbf{u}| \leq k\}$  and recall the notion of a subdifferential from convex analysis. Let  $f : \mathbb{R}^n \rightarrow \mathbb{R} \cup \{+\infty\}$  be a convex function, which may take also the  $+\infty$  values. The set

$$\begin{aligned} \partial f(\mathbf{x}) := \{ \mathbf{p} \in \mathbb{R}^n : f(\mathbf{y}) \geq f(\mathbf{x}) + \mathbf{p} \cdot (\mathbf{y} - \mathbf{x}) \quad \text{for all } \mathbf{y} \in \mathbb{R}^n \} \end{aligned}$$

is called the subdifferential of  $f$  at the point  $\mathbf{x}$ ; its elements  $\mathbf{p} \in \partial f(\mathbf{x})$  are the subgradients of  $f$  at  $\mathbf{x}$ . If  $f$  is differentiable at  $\mathbf{x}$ , then  $\partial f(\mathbf{x}) = \{\nabla f(\mathbf{x})\}$ , and if  $f(\mathbf{x}) = +\infty$ ,  $\partial f(\mathbf{x})$  is an empty set. In addition, if  $\mathbf{0} \in \partial f(\mathbf{x})$ , then  $f(\mathbf{x}) \leq f(\mathbf{y})$  for all  $\mathbf{y}$ .

It is not difficult to find the subdifferential of the indicator function of the set  $\tilde{K}$

$$I_{\tilde{K}}(\mathbf{x}) = \begin{cases} 0 & \mathbf{x} \in \tilde{K} \\ \infty & \mathbf{x} \notin \tilde{K}. \end{cases}$$

For  $\mathbf{x} \in \tilde{K}$ , we obtain  $\mathbf{p} \in \partial I_{\tilde{K}}(\mathbf{x})$  if  $\mathbf{p} \cdot (\mathbf{y} - \mathbf{x}) \leq 0$  for any  $\mathbf{y} \in \tilde{K}$ . Clearly, if  $|\mathbf{x}| < k$ , this condition holds only for  $\mathbf{p} = \mathbf{0}$ , and if  $|\mathbf{x}| = k$ ,  $\mathbf{p}$  can be any vector in the same direction as  $\mathbf{x}$ . Hence, the conditions in (5) can be written as

$$\dot{\mathbf{m}} \in \partial I_{\tilde{K}}(\mathbf{h}_i). \quad (6)$$

It follows from the definition of a subdifferential that while  $\mathbf{h}_i$  belongs to the interior of the set  $\tilde{K}$ , i.e.,  $|\mathbf{h}_i| < k$ , the

magnetization does not change:  $\dot{\mathbf{m}} = \mathbf{0}$ ; whereas, if  $|\mathbf{h}_i| = k$ , then (6) determines the unique direction of  $\dot{\mathbf{m}}$ , since  $\partial I_{\tilde{K}}(\mathbf{h}_i) = \{\mathbf{u} \in \mathbb{R}^3 : \mathbf{u} = \lambda \mathbf{h}_i, \lambda \geq 0\}$ .

Until now, the “dry-friction law” was not defined precisely. Now, we explain our choice of (5), which does not follow from (4), since it is not the only constitutive relation for which (4) holds. According to a general definition by Moreau [16, p. 64], to set a dry-friction relation between the irreversible field  $\mathbf{h}_i$  (the “friction force”) and the magnetization velocity  $\dot{\mathbf{m}}$ , it is required to define a closed convex set of admissible irreversible fields,  $\tilde{K}$ , and postulate the maximal dissipation principle: for a given  $\dot{\mathbf{m}}$ , the field  $\mathbf{h}_i$  should maximize the dissipation power  $\mu_0 \mathbf{h}_i \cdot \dot{\mathbf{m}}$  in the set  $\tilde{K}$ . Such a relation between  $\dot{\mathbf{m}}$  and  $\mathbf{h}_i$  is equivalent to (6), which is equivalent to (5).

In the anisotropic case, we also postulate that  $\dot{\mathbf{m}} \in \partial I_{\tilde{K}}(\mathbf{h}_i)$ , where now, since  $k$  is a symmetric positive-definite matrix,  $\tilde{K} := \{\mathbf{u} \in \mathbb{R}^3 : |k^{-1}\mathbf{u}| \leq 1\}$ . In this case, rewriting (4) as  $k^{-1}\mathbf{h}_i \cdot \dot{\mathbf{m}} = |k\dot{\mathbf{m}}|$ , we see that this equality holds, since  $\dot{\mathbf{m}} \in \partial I_{\tilde{K}}(\mathbf{h}_i)$  means that

$$\mathbf{h}_i \in \tilde{K} \text{ is such that } \dot{\mathbf{m}} \cdot (\mathbf{u} - \mathbf{h}_i) \leq 0 \text{ for any } \mathbf{u} \in \tilde{K} \quad (7)$$

which is equivalent to the multivalued constitutive relation

$$\begin{aligned} |k^{-1}\mathbf{h}_i| &\leq 1; \\ \text{if } |k^{-1}\mathbf{h}_i| < 1 \text{ then } \dot{\mathbf{m}} &= \mathbf{0}; \\ \text{if } \dot{\mathbf{m}} \neq \mathbf{0} \text{ then } k\dot{\mathbf{m}} \text{ has the direction of } k^{-1}\mathbf{h}_i. \end{aligned}$$

Note that if  $\mathbf{h}_i \in \tilde{K}$ , then the reversible field  $\mathbf{h}_r = \mathbf{h}(t) - \mathbf{h}_i$  belongs to the set

$$K(t) := \{\mathbf{u} \in \mathbb{R}^3 : |k^{-1}(\mathbf{h}(t) - \mathbf{u})| \leq 1\}$$

and the inequality (7) can be rewritten for  $\mathbf{h}_r$

$$\mathbf{h}_r \in K(t) \text{ is such that}$$

$$\dot{\mathbf{m}} \cdot (\mathbf{u} - \mathbf{h}_r) \geq 0 \text{ for any } \mathbf{u} \in K(t). \quad (8)$$

Inverting the dependence  $\mathbf{h}_r = \mathbf{f}(\mathbf{m})$ , we obtain that  $\mathbf{m} = f^{-1}(\mathbf{h}_r)$ , and as in [7], assume further that the vectors  $\mathbf{h}_r$  and  $\mathbf{m}$  are parallel, i.e.,  $\mathbf{m} = M_{an}(\mathbf{h}_r)(\mathbf{h}_r/h_r)$ , where the anhysteretic function  $M_{an}$  is nondecreasing and  $M_{an}(0) = 0$ .

Let  $S(\mathbf{u}) = \int_0^u M_{an}(s)ds$ . Then

$$\mathbf{m} = \nabla S(\mathbf{h}_r). \quad (9)$$

To solve (8) and (9) numerically, we substitute (9) into the discretized version of (8)

$$\mathbf{h}_r \in K(t) \text{ is such that}$$

$$(\mathbf{m} - \check{\mathbf{m}}) \cdot (\mathbf{u} - \mathbf{h}_r) \geq 0 \text{ for any } \mathbf{u} \in K(t)$$

where “ $\check{\cdot}$ ” means the value from the previous time level. This yields the variational inequality

$$\text{find } \mathbf{h}_r \in K(t) \text{ such that}$$

$$(\nabla S(\mathbf{h}_r) - \check{\mathbf{m}}) \cdot (\mathbf{u} - \mathbf{h}_r) \geq 0 \text{ for any } \mathbf{u} \in K(t) \quad (10)$$

which is equivalent to an optimization problem:  $\mathbf{h}_r(t)$  is a solution of

$$\min_{\mathbf{u} \in K(t)} \{S(\mathbf{u}) - \check{\mathbf{m}} \cdot \mathbf{u}\}. \quad (11)$$

It can be shown that if the derivative  $M'_{an} > 0$ , then  $S$  is a strictly convex function, and since the set  $K(t)$  is convex, (11) has a unique solution.

The unconstrained minimum of  $S(\mathbf{u}) - \check{\mathbf{m}} \cdot \mathbf{u}$  is at a point  $\mathbf{u}$ , where  $\nabla S(\mathbf{u}) - \check{\mathbf{m}} = 0$ ; in this case,  $\mathbf{u} = \check{\mathbf{h}}_r$ . Hence, if  $|k^{-1}(\mathbf{h}(t) - \check{\mathbf{h}}_r)| \leq 1$ , this is a solution also to the constrained problem (11) and  $\mathbf{m} = \check{\mathbf{m}}$ . Otherwise, the equality constraint  $|k^{-1}(\mathbf{h}(t) - \mathbf{h}_r(t))| = 1$  holds. We use this observation to solve the optimization problem (11) numerically as follows.

At each time level, the solution to (11) is  $\mathbf{h}_r(t) = \check{\mathbf{h}}_r$  if  $|k^{-1}(\mathbf{h}(t) - \check{\mathbf{h}}_r)| \leq 1$ . In 2-D problems, if this inequality is not true,  $\mathbf{h}_r = \mathbf{h}(t) + k\mathbf{i}_\phi$ , where  $\mathbf{i}_\phi = (\cos \phi, \sin \phi)$  is a unit vector, and therefore, one is required to solve an unconstrained 1-D minimization problem

$$\min_\phi \{S(\mathbf{h}(t) + k\mathbf{i}_\phi) - \check{\mathbf{m}} \cdot (\mathbf{h}(t) + k\mathbf{i}_\phi)\}. \quad (12)$$

Although there can be several local minima, a good initial approximation to the optimal direction  $\phi$  is the direction of the vector  $k^{-1}(\check{\mathbf{h}}_r - \mathbf{h}(t))$ . Starting from this approximation, we solved the problem  $g'(\phi) = 0$ , where  $g(\phi) = S(\mathbf{h}(t) + k\mathbf{i}_\phi) - \check{\mathbf{m}} \cdot (\mathbf{h}(t) + k\mathbf{i}_\phi)$ , efficiently using Newton's method (see Appendix A). Usually, two or three iterations of this method have been sufficient to find the solution with high accuracy. Although we have only solved 2-D problems, this method should be efficient also in 3-D problems, where the optimal direction is determined by two angles.

We note that in [7]–[12], [14], and [15], the vector

$$\mathbf{h}_r = \mathbf{h} + k \frac{\check{\mathbf{h}}_r - \mathbf{h}(t)}{|\check{\mathbf{h}}_r - \mathbf{h}(t)|} \quad (13)$$

is chosen (in the isotropic case) as the new value of  $\mathbf{h}_r$  if  $|\mathbf{h}(t) - \check{\mathbf{h}}_r| > k$ . This is equivalent to using our initial approximation for  $\phi$  without any further correction and turns (8), (9) into a vector play model. In the vectorial case, such an approach can introduce an error that does not disappear as the increments of  $\mathbf{h}$  tend to zero (see the following).

The hysteresis model (8) and (9) is oversimplified, but it will be used as a building block for a more realistic model (Section III). First, it seems instructive to illustrate the behavior of this model by several examples. Let us assume, as in [7], that

$$M_{an}(h_r) = \frac{2m_s}{\pi} \arctan \left( \frac{h_r}{A} \right) \quad (14)$$

where  $m_s$  is the saturation magnetization and the parameter  $A$  determines the steepness of the curve. Another popular representation of the anhysteretic curve [10], [11], [23] is the Langevin function  $M_{an}(h_r) = m_s [\coth(h_r/B) - B/h_r]$ , which is very well approximated by (14) if  $A = 1.7B$ . In general, the curve can be approximated by a spline (and we will use a spline representation of  $M_{an}$  to model nonoriented electrical steel in Section IV). We found that for  $m_s = 1.23 \cdot 10^6$  A/m,  $A = 38$  A/m, and  $k = 71$  A/m, the model (8) and (9) with (14) describes well the major hysteresis loop shown in [15, Fig. 5] (here  $k$  determines the loop width, which is almost constant except close to saturation, where it quickly drops to zero).

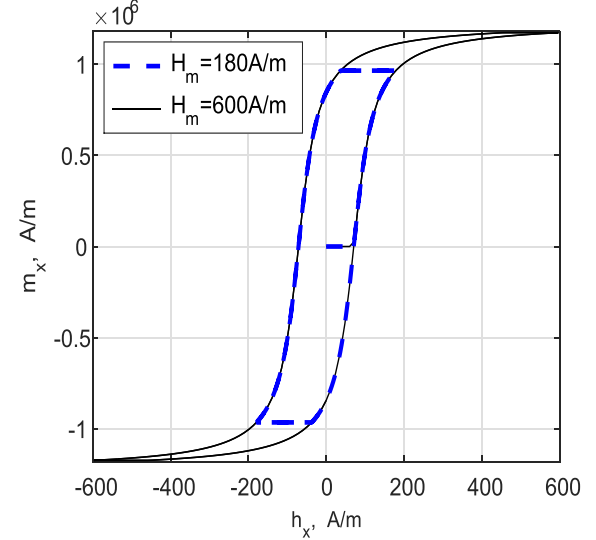


Fig. 1. Two hysteresis loops—simplified model;  $\mathbf{h} = (H_m \sin t, 0)$ .

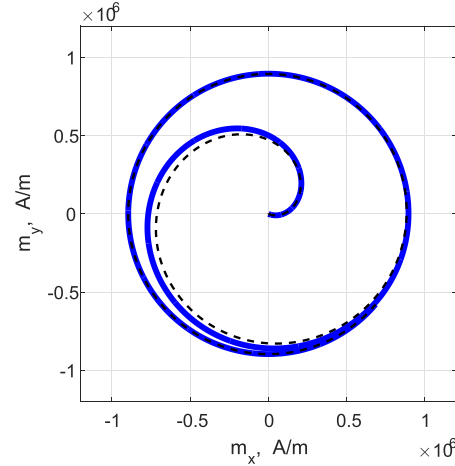


Fig. 2. Model solution  $\mathbf{m} = (m_x, m_y)$  (solid line) and the explicit approximation (13) (dashed line);  $\mathbf{h} = H_m(t)(\cos t, \sin t)$ , where  $H_m(t) = 110 \min(t/6\pi, 1)$  A/m and  $k = 71$  A/m.

Let  $\mathbf{m}(0) = \mathbf{0}$ . First, we set  $\mathbf{h} = (H_m \sin t, 0)$ . This example is 1-D, the approximation (13) does not introduce any error, and, furthermore, the problem (12) can be solved analytically. We used it to check our optimization procedure. Here, and throughout this section and in Section III, the time step is chosen sufficiently small, about 200–400 time steps per cycle, so that the shown figures are independent of the time step.

The simulation results for two values of the amplitude  $H_m$  (Fig. 1) show that, although the model's prediction of the major hysteresis loop is correct, the minor loop and the initial magnetization curve are unrealistic.

In our next example (Fig. 2), we assume that the magnetic field rotates,  $\mathbf{h} = H_m(t)(\cos t, \sin t)$ , with the amplitude  $H_m(t) = 110 \min(t/6\pi, 1)$  growing with time until its maximal value 110 A/m is reached. This is a nonscalar situation and we compare the accurate numerical solution of (12), equivalent to the time discretized version of (8), to the explicit, at each time step, discretized vector play model based on the approximation (13). Although the solutions are different in

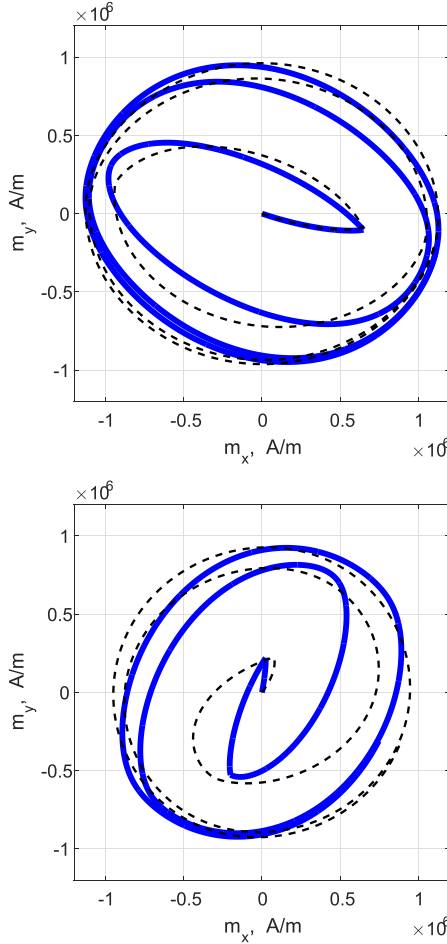


Fig. 3. Similar to Fig. 2 except for  $\mathbf{h} = H_m(t)(3 \cos t, \sin t)$  (top) and for an anisotropic material characterized by the diagonal matrix  $k = \text{diag}(71, 35.5)$  A/m (bottom).

the transient regime, the difference is small and disappears soon after the amplitude of the rotating magnetic field becomes constant. However, the approximation (13) is less accurate if the amplitudes of the magnetic field components  $h_x$  and  $h_y$  are different [Fig. 3 (top)] or the material is anisotropic [Fig. 3 (bottom)].

### III. MORE REALISTIC COMPOSITE MODEL OF A FERROMAGNETIC MATERIAL

Prior to using the described energy-based dry-friction-like model for modeling hysteresis in real ferromagnets, this model should be made more realistic. The main modifications, at least partially implemented in all works where such a model has been used, have been suggested already in [7] and [8]; their analogs can also be found in some previous models of hysteresis.

First, instead of a single value of the “friction coefficient”  $r$ , the material can be characterized by a distribution of  $r$  values with the volume density  $\omega(r)$ ; this approach corresponds better to the statistical distribution of the pinning center strengths in the ferromagnetic microstructure. The total magnetization is  $\mathbf{m} = \int \mathbf{m}' \omega(r) dr$ , where each moment  $\mathbf{m}'(t)$  obeys the dry-friction model with its own value of  $r$ . This can improve the description of the initial magnetization curve and the minor loops.

For numerical simulations, we approximate the distribution by a mixture of  $N$  types of pseudoparticles with volume fractions  $\omega^l > 0$ , satisfying  $\sum_{l=1}^N \omega^l = 1$ . Each type is characterized by its own  $r = r^l$  and to account for partial reversibility of the material response [7], [12], we assign  $r = 0$  to one of the pseudoparticle types. Overall, we assume

$$\begin{aligned} W &= \frac{1}{2} \mu_0 h^2 + \sum_{l=1}^N \omega^l U(\mathbf{m}^l) \\ \mathbf{b} &= \mu_0 \left( \mathbf{h} + \sum_{l=1}^N \omega^l \mathbf{m}^l \right) \\ \dot{W} &= \mathbf{h} \cdot \dot{\mathbf{b}} - \sum_{l=1}^N \omega^l |r^l \dot{\mathbf{m}}^l| \end{aligned}$$

and arrive at an analog of (3)

$$\sum_{l=1}^N \omega^l \{(\mathbf{h} - \mathbf{f}(\mathbf{m}^l)) \cdot \dot{\mathbf{m}}^l - |k^l \dot{\mathbf{m}}^l|\} = 0 \quad (15)$$

where  $k^l = (1/\mu_0)r^l$  and, as before,  $\mathbf{f} = (1/\mu_0)\nabla U$ . We set  $\mathbf{h}_r^l = \mathbf{f}(\mathbf{m}^l)$ ,  $\mathbf{h}_i^l = \mathbf{h} - \mathbf{h}_r^l$  and, similar to what was done above, satisfy (15) by postulating the constitutive relations

$$\dot{\mathbf{m}}^l \in \partial I_{\tilde{K}^l}(\mathbf{h}_i^l)$$

where

$$\tilde{K}^l := \{\mathbf{u} \in \mathbb{R}^3 : |(k^l)^{-1}\mathbf{u}| \leq 1\};$$

if  $k^l = 0$ , we assume  $\tilde{K}^l := \{\mathbf{0}\}$ . As before, we reformulate these conditions as variational inequalities, similar to (8) and (9). After discretization in time, these inequalities become equivalent to optimization problems similar to (11): we find  $\mathbf{h}_r^l$  on a new time level as a solution to

$$\min_{\mathbf{u} \in K^l(t)} \{S(\mathbf{u}) - \dot{\mathbf{m}}^l \cdot \mathbf{u}\} \quad (16)$$

where

$$K^l(t) := \{\mathbf{u} \in \mathbb{R}^3 : |(k^l)^{-1}(\mathbf{h}(t) - \mathbf{u})| \leq 1\}$$

except for  $k^l = 0$ : in that case,  $K^l(t) := \{\mathbf{h}(t)\}$ . Finally, we compute  $\mathbf{m}^l = \mathbf{f}^{-1}(\mathbf{h}_r^l) = M_{an}(\mathbf{h}_r^l)(\mathbf{h}_r^l/h_r^l)$  and  $\mathbf{m} = \sum_{l=1}^N \omega^l \mathbf{m}^l$ . As an example, we simulated several hysteresis loops (Fig. 4) for a material characterized by the anhysteretic function (14) with  $m_s = 1.23 \cdot 10^6$  A/m,  $A = 50$  A/m, and represented by  $N = 20$  pseudoparticle types with  $k^l = 140(l-1)/(N-1)$  A/m, each having the same volume fraction  $\omega^l = 1/N$ .

As was noted in [7], it may be better to assume that the magnetization of a pseudoparticle does not evolve independently but is influenced by the other particles. Hence, as the second essential modification of his model, Bergqvist replaced the “driving force” of this evolution,  $\mathbf{h}(t)$ , by the “effective” field  $\mathbf{h}(t) + \alpha \mathbf{m}(t)$ , where  $\alpha$  is a material-dependent parameter. Such effective fields are often employed also in other models of hysteresis [1], [2], [22]; an explanation of the interaction term  $\alpha \mathbf{m}(t)$  was presented in [17, Ch. 4].

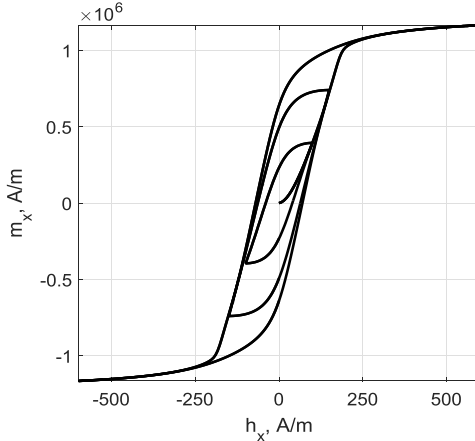


Fig. 4. Simulation using the composite model.

With this modification, the convex time-dependent sets  $K^l(t)$  should be replaced by

$$K^l(t, \mathbf{m}) := \{\mathbf{u} \in \mathbb{R}^3 : |(k^l)^{-1}(\mathbf{u} - \mathbf{h}(t) - \alpha\mathbf{m})| \leq 1\}$$

if  $k^l \neq 0$  and  $K^l(t, \mathbf{m}) := \{\mathbf{h}(t) + \alpha\mathbf{m}\}$  otherwise. The internal variables  $\mathbf{h}_r^l$  are now solutions of the optimization problems

$$\min_{\mathbf{u} \in K^l(t, \mathbf{m})} \{S(\mathbf{u}) - \dot{\mathbf{m}}^l \cdot \mathbf{u}\} \quad (17)$$

in which the constraints depend on the unknown solution itself, since

$$\mathbf{m} = \sum_{l=1}^N \omega^l \mathbf{m}^l = \sum_{l=1}^N \omega^l M_{an}(h_r^l) \frac{\mathbf{h}_r^l}{h_r^l}$$

The implicit constraints in (17) complicate the determination of the magnetizations  $\mathbf{m}^l$  (such problems are equivalent to quasi-variational inequalities). Nevertheless, an efficient iterative method can be proposed (see Section V).

Further modification of the model is needed to account for the known phenomenon of zero hysteresis loss in a rotational field at saturation [17], [18]. To describe this “saturation property,” it was suggested [7], [15], [19] to replace the constant intrinsic coercivity of each pseudoparticle,  $k^l$ , by a decreasing function  $k^l(h_r^l)$  attaining zero at a saturation value  $h_r^l = h_s$ . In [15] and [19], however, only a “monoparticle” model with the approximate update rule (13) has been considered. We suppose that in a composite model, the lossless coherent rotation of all magnetization vectors  $\mathbf{m}^l$  is, probably, better described if, for all  $l$ ,  $k^l = k^l(m)$ , which simultaneously drop to zero as the total magnetization  $m$  reaches saturation. In this paper, however, we consider for simplicity only constant  $k^l$  values.

#### IV. IDENTIFICATION OF THE PARAMETERS IN THE MODEL

The practical implementation of the phenomenological model described above needs identification of the anhysteretic curve  $M_{an}$ , the material parameter  $\alpha$ , the coefficients  $k^l$  (scalar or matrices, constant or dependent on  $m$ ), and the corresponding weights  $\omega^l$ ,  $l = 1, \dots, N$ . Of course, the identification of parameters is needed also for other models of hysteresis and a variety of approaches have been proposed; the identification procedure depends on the model and the experimental data available.

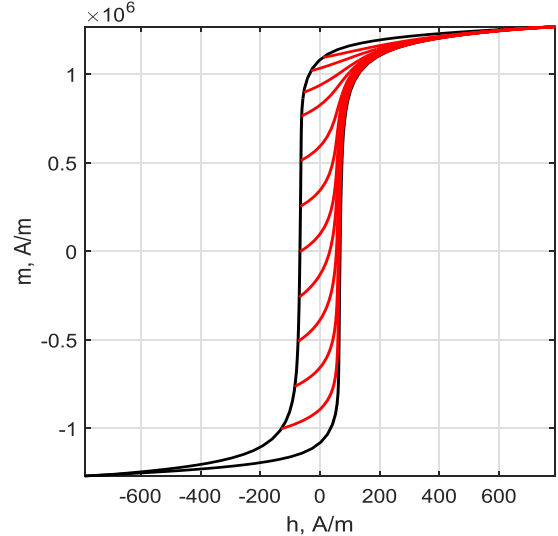


Fig. 5. Hysteresis curves—experimental.

Here, we present a consistent algorithm for the identification of the parameters in the model for a nonoriented steel using the experimental major hysteresis loop and 11 FORCs (the 1.8% Si steel N3 in [20] (Fig. 5); see also [21]). Because of the symmetry, only the ascending part of the major loop was used; this curve was regarded as an additional FORC that starts at a strong negative magnetic field  $-800$  A/m. We assume that the material is isotropic (in the anisotropic case, similar measurements along the main material axes should be used for the identification) and, for simplicity, seek constant scalar values for  $k^l$ ,  $l = 1, \dots, N$ . Postulating that  $N = 41$  possible  $k^l$  values are uniformly distributed from zero to  $800$  A/m with the step  $20$  A/m, we need to find only the appropriate weights  $\omega^l$  to specify the distribution of the pseudoparticles.

No specific formulas were assumed for the anhysteretic function  $M_{an}(|\mathbf{u}|)$ : this function was approximated by a cubic spline with the “not-a-knot” end conditions as follows. First, we determined the interval, in which this function needs to be defined. Although the measured magnetic field did not exceed  $800$  A/m, the reversible fields  $\mathbf{h}_r^l$  driven by the effective field  $\mathbf{h}_{eff} = \mathbf{h} + \alpha\mathbf{m}$  can be out of this range. After several tests needed to estimate, at least crudely at first, the value of  $\alpha$  (see below), we chose to approximate this function in the interval  $[0, 1750]$  A/m. The anhysteretic function was then sought as a cubic spline with a fixed set of equidistant knots:  $250i$  A/m,  $i = 0, 1, \dots, 7$ . Since  $M_{an}(0) = 0$  is fixed, the spline is determined by its *a priori* unknown values  $M_i$  at the seven other knots. Note that in this experiment, the fields can be regarded as scalar. In such a case, let  $h$  denote the field itself (which may be negative) and not its magnitude  $|h|$  as above.

Let the anhysteretic function  $M_{an}$ , the particle fractions  $\omega^l$ , and the parameter  $\alpha$  be given. At any point  $\{h_0, m_0\}$  on the descending branch of the major hysteresis loop, we know the internal state  $\mathbf{h}_r^l$  of all pseudoparticle types:  $\mathbf{h}_r^l(h_0) = h_0 + \alpha m_0 + k^l$ . If at this point the magnetic field starts to grow, the particle state evolution along the FORC  $\{h, m(h)\}$  thus created can be described as  $\mathbf{h}_r^l(h) = \max\{\mathbf{h}_r^l(h_0), \mathbf{h} + \alpha m(h) - k^l\}$ . The model prediction for the total magnetization along this curve,

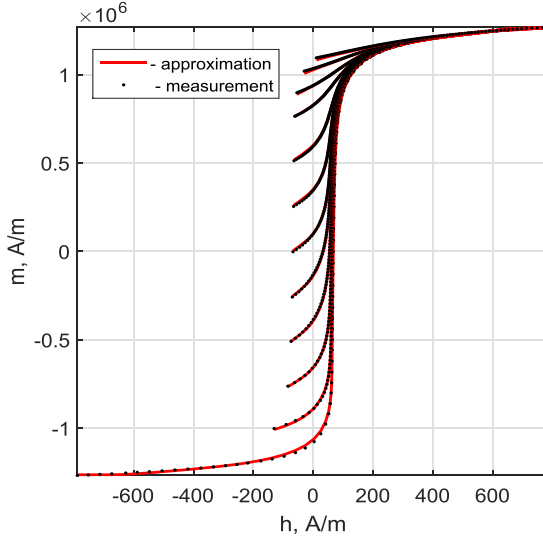


Fig. 6. Least-squares fit of the FORCs.

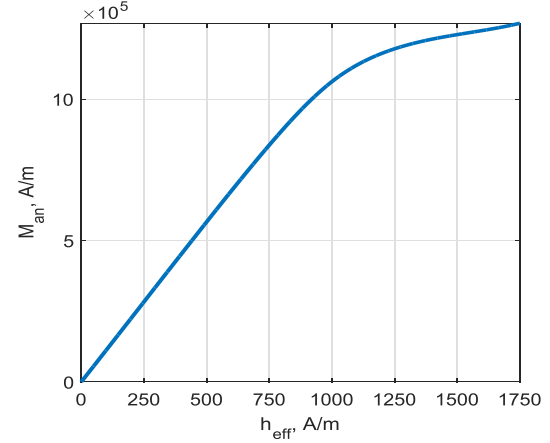
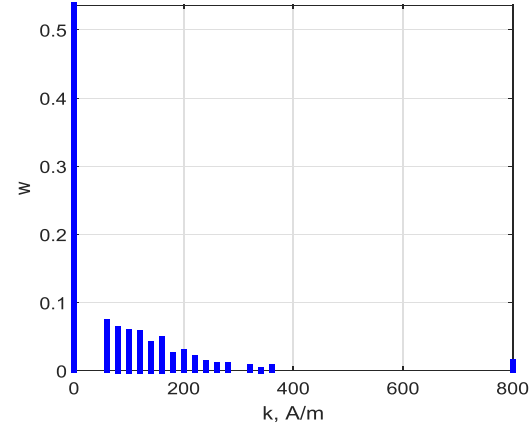
$\mathcal{M}(h) = \sum_{l=1}^N \omega^l M_{an}(h_r^l(h))$ , can be compared with the measured  $m^*(h)$  values for the same FORC. Our identification procedure finds the parameters  $M_i$  of  $M_{an}$ , the weights  $\omega^l$  and  $\alpha$  minimizing the least-squares method residual, i.e. the sum  $L$  of  $[\mathcal{M}(h) - m^*(h)]^2$  over all measured points on all experimental FORCs. Efficient standard functions of MATLAB were used in our three-level optimization algorithm as follows.

On the lowest level, the program determines the weights  $\omega^l$  satisfying  $\omega^l \geq 0$ ,  $\sum_{l=1}^N \omega^l = 1$  and minimizing the least-squares residual  $L$  for the given values of  $M_i$  and  $\alpha$ . This is a quadratic programming problem solved by the `lsqlin` function from the MATLAB Optimization toolbox 7.2. On the next level, the MATLAB function `fminunc` realizes the unconstrained minimization over the set of  $M_i$  for a given value of  $\alpha$ . Plotting the resulting function  $L = L(\alpha)$  helped us to crudely estimate the position of the minimum, and on the upper level, this information was used by the MATLAB function `fminbnd` to find the optimal value of  $\alpha$ ; the corresponding  $M_i$ ,  $\omega^l$  were thereby also obtained. Minimization of this function on a standard PC takes about 10 min.

Although we did not consider any possible dependence of  $k^l$  on  $\mathbf{m}$ , a very good fit of the experimental curves has been obtained for  $\alpha = 8.8 \cdot 10^{-4}$  (Fig. 6); the anhysteretic function  $M_{an}$  and the weights  $\omega^l$  are shown in Figs. 7 and 8, respectively. We note that for only 17 of the 41 predefined values of  $k^l$  did the identified volume fractions  $\omega^l$  exceed  $10^{-3}$ . Only these pseudoparticles are considered in our finite-element computations below; their total fraction is 0.9991. The results obtained show that for this material, the reversible magnetization dominates (see Fig. 8), and there is a very significant reciprocal influence of pseudoparticles through the  $\alpha\mathbf{m}$  term in  $\mathbf{h}_{eff}$  (see Figs. 5 and 7): without this term, the  $M_{an}(h)$  curve would be a much steeper line between the ascending and descending branches of the main hysteresis loop.

## V. NUMERICAL SCHEME FOR A 2-D HYSTERESIS AND EDDY CURRENT PROBLEM

Let us consider a long ferromagnetic cylinder, parallel to the  $z$ -axis and having a cross section  $\Omega$ , carrying a transport

Fig. 7. Anhysteretic function  $M_{an}$ .Fig. 8. Weights  $\omega(k)$ —identification result.

current  $I(t)$  and placed into a perpendicular uniform external field  $\mathbf{h}_e(t)$ . The electric field  $\mathbf{e}(x, y, t)$  and the current density  $\mathbf{j}(x, y, t)$  are parallel to the  $z$ -axis; we can also choose the vector magnetic potential  $\mathbf{a}(x, y, t)$  parallel to the  $z$ -axis (so that  $\nabla \cdot \mathbf{a} = 0$ ). Hence, these variables can be regarded as scalar and we will use the scalar notation  $e$ ,  $j$  and  $a$  (which should not be confused with the absolute values of these vectors). The vector fields  $\mathbf{h}(x, y, t)$ ,  $\mathbf{b}(x, y, t)$  and  $\mathbf{m}(x, y, t)$  are parallel to the  $xy$  plane.

We will use a 2-D eddy current and magnetization problem formulation, similar to that proposed for 3-D problems with hysteresis in [23], but employ the Bergqvist model for magnetization discussed above. This model should be incorporated as a local constitutive relation

$$\mathbf{m} = \mathbf{M}[\mathbf{h}_{eff}] \quad (18)$$

where  $\mathbf{h}_{eff} = \mathbf{h} + \alpha\mathbf{m}$  and  $\mathbf{h} = (1/\mu_0)\mathbf{b} - \mathbf{m} = (1/\mu_0)\nabla \times \mathbf{a} - \mathbf{m}$ . Here (and in the following), square brackets are used for the operator argument and  $\nabla \times \mathbf{a} = (\partial_y a, -\partial_x a)$ . The value  $\mathbf{M}[\mathbf{h}_{eff}]$  at a point depends on the history of  $\mathbf{h}_{eff}$  at this point: implicitly, the local operator  $\mathbf{M}$  keeps track of the state of the internal variables  $\mathbf{h}_r^l$  and  $\mathbf{m}^l$ . The density of the power loss due to magnetization is  $W_H = \mu_0 \sum_{l=1}^N \omega^l |k^l \mathbf{m}^l|$ . Ohm's law  $e = \rho j$ , where  $\rho$  is the resistivity, is another constitutive relation characterizing the material. The density of the eddy and transport current loss is  $W_E = \rho j^2$ . We note that the

so-called anomalous or excess loss, attributed to microscopic eddy currents caused by small, almost instantaneous jumps of domain walls (the Barkhausen noise), is not described by this model. As is shown in [24], for the nonoriented steel considered in Section IV, this loss is small, at least for the magnetization in the rolling direction; for other magnetization directions, the excess loss can, possibly, reach 10%–20% of the total loss [20].

For the specified geometry and gauge, the electric field can be written as  $e = -\partial_t a + c(t)$ , where the time-dependent constant  $c(t)$  results from the parallel to the  $z$ -axis gradient of the scalar potential,  $\nabla \Phi$  [25]. This yields that

$$\rho j = -\partial_t a + c(t) \quad (19)$$

where the unknown time-dependent constant  $c(t)$  is determined implicitly by the given transport current

$$\int_{\Omega} j d\mathbf{r} = I(t). \quad (20)$$

In our numerical simulations, we will assume that  $I(t) = 0$ .

The vector potential can be represented as a sum,  $a = a_e + a_j + a_m$ , of the potentials associated with the external field, current density, and magnetization, respectively. Here,  $a_e = \mu_0(y h_{e,x} - x h_{e,y})$  and from [26]

$$a_j[j] = \mu_0 \int_{\Omega} G(\mathbf{r} - \mathbf{r}') j(\mathbf{r}', t) d\mathbf{r}' \quad (21)$$

$$a_m[\mathbf{m}] = \mu_0 \int_{\Omega} \nabla G(\mathbf{r} - \mathbf{r}') \times \mathbf{m}(\mathbf{r}', t) d\mathbf{r}' \quad (22)$$

where  $\nabla$  is the gradient with respect to  $\mathbf{r} = (x, y)$  and  $G(\mathbf{r}) = (1/2\pi) \ln(1/|\mathbf{r}|)$  is Green's function.

Correspondingly, the magnetic field can be represented as the sum:  $\mathbf{h} = \mathbf{h}_e + \mathbf{h}_j + \mathbf{h}_m$ , where

$$\begin{aligned} \mathbf{h}_j[j] &= \int_{\Omega} \nabla G(\mathbf{r} - \mathbf{r}') \times j(\mathbf{r}', t) d\mathbf{r}' \\ &= \left( \int_{\Omega} j(\mathbf{r}', t) \partial_y G(\mathbf{r} - \mathbf{r}') d\mathbf{r}' \right. \\ &\quad \left. - \int_{\Omega} j(\mathbf{r}', t) \partial_x G(\mathbf{r} - \mathbf{r}') d\mathbf{r}' \right) \end{aligned}$$

and see<sup>1</sup>

$$\begin{aligned} \mathbf{h}_m[\mathbf{m}] &= \frac{1}{\mu_0} \mathbf{b}_m - \mathbf{m} \\ &= \nabla \int_{\Omega} \nabla \cdot [G(\mathbf{r} - \mathbf{r}') \mathbf{m}(\mathbf{r}', t)] d\mathbf{r}'. \end{aligned} \quad (23)$$

<sup>1</sup>To find  $\mathbf{b}_m = \nabla \times \mathbf{a}_m$ , we note that

$$\begin{aligned} &\nabla \times [\nabla G(\mathbf{r} - \mathbf{r}') \times \mathbf{m}(\mathbf{r}', t)] \\ &= -\mathbf{m}(\mathbf{r}', t)(\Delta G) + \nabla G(\nabla \cdot \mathbf{m}(\mathbf{r}', t)) \\ &\quad - (\nabla G \cdot \nabla) \mathbf{m}(\mathbf{r}', t) + (\mathbf{m}(\mathbf{r}', t) \cdot \nabla) \nabla G \\ &= \mathbf{m}(\mathbf{r}', t) \delta(\mathbf{r} - \mathbf{r}') + \nabla [\nabla \cdot [G(\mathbf{r} - \mathbf{r}') \mathbf{m}(\mathbf{r}', t)]] \end{aligned}$$

Hence

$$\begin{aligned} &\nabla \times \int_{\Omega} \nabla G(\mathbf{r} - \mathbf{r}') \times \mathbf{m}(\mathbf{r}', t) d\mathbf{r}' \\ &= \mathbf{m}(\mathbf{r}, t) + \nabla \int_{\Omega} \nabla \cdot [G(\mathbf{r} - \mathbf{r}') \mathbf{m}(\mathbf{r}', t)] d\mathbf{r}'. \end{aligned}$$

The main unknowns in this model are  $\mathbf{m}(\mathbf{r}, t)$  and  $j(\mathbf{r}, t)$ : provided that these variables are found,  $\mathbf{h}$  and  $\mathbf{b}$  can also be calculated;  $c(t)$  is an auxiliary unknown. After discretization in time, the problem to be solved on each time level  $n$  consists of three linear equations

$$\begin{aligned} \tau \rho j^n + a_j[j^n] + a_m[\mathbf{m}^n] - \tau c^n \\ = a_e^{n-1} - a_e^n + a_j[j^{n-1}] + a_m[\mathbf{m}^{n-1}] \end{aligned} \quad (24)$$

$$\int_{\Omega} j^n d\mathbf{r} = I^n \quad (25)$$

$$\mathbf{h}_{\text{eff}}^n = \mathbf{h}_e^n + \mathbf{h}_j[j^n] + \mathbf{h}_m[\mathbf{m}^n] + \alpha \mathbf{m}^n \quad (26)$$

where  $\tau$  is the time step, supplemented by the nonlinear relationship

$$\mathbf{m}^n = \mathbf{M}[\mathbf{h}_{\text{eff}}^n]. \quad (27)$$

Our iterative scheme was based on the representation

$$\mathbf{m}^{n,k+1} = \mathbf{M}[\mathbf{h}_{\text{eff}}^{n,k}] + D[\mathbf{h}_{\text{eff}}^{n,k}] (\mathbf{h}_{\text{eff}}^{n,k+1} - \mathbf{h}_{\text{eff}}^{n,k}) \quad (28)$$

where  $k$  is the iteration number and  $D[\mathbf{u}]$  is, at each point of  $\Omega$ , the  $2 \times 2$  matrix of partial derivatives

$$D[\mathbf{u}] = \begin{pmatrix} \partial_{u_x} M_x[\mathbf{u}] & \partial_{u_y} M_x[\mathbf{u}] \\ \partial_{u_x} M_y[\mathbf{u}] & \partial_{u_y} M_y[\mathbf{u}] \end{pmatrix}.$$

Since the analytical calculation of these derivatives is difficult, we used their numerical approximations: replacing  $u_x$  by  $u_x \pm \Delta$ , and keeping  $u_y$  unchanged, we used the central difference to estimate  $\partial_{u_x} M[\mathbf{u}]$ , similarly for  $\partial_{u_y} M[\mathbf{u}]$ .

Substituting (28) into (24) and (26) yields a linear system for  $\mathbf{h}_{\text{eff}}^{n,k+1}$ ,  $j^{n,k+1}$ , and  $c^{n,k+1}$ . These iterations should be repeated until convergence of  $\mathbf{h}_{\text{eff}}^n$  with a given tolerance; the magnetization and the magnetic field in the magnetic material are then found as  $\mathbf{m}^n = \mathbf{M}[\mathbf{h}_{\text{eff}}^n]$  and  $\mathbf{h}^n = \mathbf{h}_{\text{eff}}^n - \alpha \mathbf{m}^n$ , respectively.

The described iterative procedure has been applied to the finite-element approximation of this problem. We triangulated the domain  $\Omega$  and used piecewise constant approximations for all variables,  $j$ ,  $a$ ,  $\mathbf{h}$ , and  $\mathbf{m}$ . The finite-element approximation of the integral operator equation (24) involves the computation of matrices with the entries [see (21) and (22)]

$$L_{e,e'} = \int_e \int_{e'} G(\mathbf{r} - \mathbf{r}') d\mathbf{r}' d\mathbf{r} \quad (29)$$

$$L_e^x = \int_e \int_{e'} \partial_x G(\mathbf{r} - \mathbf{r}') d\mathbf{r}' d\mathbf{r} \quad (30)$$

$$L_e^y = \int_e \int_{e'} \partial_y G(\mathbf{r} - \mathbf{r}') d\mathbf{r}' d\mathbf{r} \quad (31)$$

for each pair of triangles  $e$ ,  $e'$ . Only the matrices  $L^x$ ,  $L^y$  defined above are needed to find  $\mathbf{h}_j[j]$  in (26). However, to compute the  $\mathbf{h}_m[\mathbf{m}]$  part of  $\mathbf{h}_{\text{eff}}$ , one needs [see (23)] matrices with entries

$$L_{e,e'}^{xx} = \int_e \int_{e'} \partial_{xx}^2 G(\mathbf{r} - \mathbf{r}') d\mathbf{r}' d\mathbf{r} \quad (32)$$

$$L_{e,e'}^{yy} = \int_e \int_{e'} \partial_{yy}^2 G(\mathbf{r} - \mathbf{r}') d\mathbf{r}' d\mathbf{r} \quad (33)$$

$$L_{e,e'}^{xy} = L_{e,e'}^{yx} = \int_e \int_{e'} \partial_{xy}^2 G(\mathbf{r} - \mathbf{r}') d\mathbf{r}' d\mathbf{r}. \quad (34)$$

Some of the integrals in (29)–(34) are singular; their computation is described in Appendix B. We note that the matrices  $L$ ,  $L^{xx}$ ,  $L^{xy}$ , and  $L^{yy}$  are symmetric, whereas the  $L^x$ ,  $L^y$  are antisymmetric.

To approximate the matrix  $D$  in each element, we used  $\Delta = 2 \cdot 10^{-6} \max(1, h)$ . Convergence of the iterations was stable and fast: three to five iterations per time level ensured convergence with the relative tolerance  $10^{-6}$  (in the  $L^1$  norm) in all our simulations.

## VI. SIMULATION RESULTS

In all numerical simulations below, we assumed that the material is isotropic and used the hysteresis model parameters identified for a nonoriented steel in Section IV. As our first example, we considered a cylinder with a circular cross section  $\Omega = \{r : r < r_0\}$ . We made the eddy current negligible by choosing a very high resistivity  $\rho$ . Then, for a material with constant magnetic permeability  $\mu$ , the magnetic field can be expressed through the scalar magnetic potential,  $\mathbf{h} = -\nabla\psi$ , satisfying the Laplace equation  $(1/r)(\partial/\partial r)(r(\partial\psi/\partial r)) + (1/r^2)(\partial^2\psi/\partial\theta^2) = 0$  inside and outside the domain  $\Omega$  with the interface conditions

$$\psi|_{r_0-} = \psi|_{r_0+}, \quad \mu \frac{\partial\psi}{\partial r}\Big|_{r_0-} = \mu_0 \frac{\partial\psi}{\partial r}\Big|_{r_0+}$$

and the boundary condition  $-\nabla\psi \rightarrow \mathbf{h}_e$  as  $r \rightarrow \infty$ . Solving this problem by separation of variables, one finds that inside the cylinder the fields  $\mathbf{h}$  and  $\mathbf{m}$  are uniform

$$\mathbf{h} = \frac{2\mathbf{h}_e}{\mu_r + 1}, \quad \mathbf{m} = \frac{2\mathbf{h}_e(\mu_r - 1)}{\mu_r + 1} \quad (35)$$

where  $\mu_r = \mu/\mu_0$ . For a circular ferromagnetic cylinder, we now assume the virgin initial state ( $\mathbf{m}^l|_{t=0} = 0$  for all  $l$ ) and a uniform external field  $\mathbf{h}_e(t)$  growing from zero monotonically in a fixed direction. In this case,  $\mathbf{h}$  and  $\mathbf{m}$  are also uniform in  $\Omega$ , but obey (35) with an unknown relative permeability  $\mu_r$  varying with  $h_e$ . For this unidirectional situation, the model (18) employed predicts

$$\mathbf{m} = \sum_{l=1}^N \omega^l M_{an}([h + \alpha m - k^l]_+) \quad (36)$$

where  $u_+ = \max\{u, 0\}$ . Substituting relations (35) into (36), we arrive at a nonlinear algebraic equation for  $\mu_r$ , which is easy to solve numerically; this determines  $h$  and  $m$  for any given  $h_e$ .

This solution does not depend on  $r_0$  and was used as a partial test for our finite-element simulations. We set  $\mathbf{h}_e = (10^3 t, 0)$  A/m and used two finite-element meshes (742 and 2436 triangles) to compute the solution at  $t = 100$  s. For the crude mesh, the relative errors of our finite-element solution (in the  $L^1$  norm) did not exceed  $\delta_h = 0.08\%$  and  $\delta_m = 0.21\%$  for  $\mathbf{h}$  and  $\mathbf{m}$ , respectively; for the finer mesh, we obtained  $\delta_h = 0.05\%$  and  $\delta_m = 0.18\%$ . The moderate accuracy gain for  $\mathbf{m}$  for the finer mesh probably indicates that a nonnegligible part of the error is induced by the use of numerical integration in (29)–(34). We found that in this example, the accuracy was practically independent

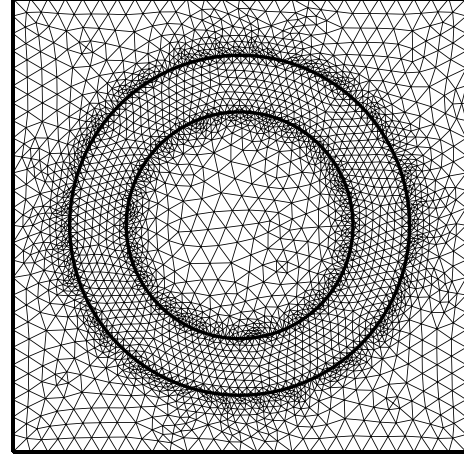


Fig. 9. Finite-element mesh.

of the constant time step  $\tau$ ; such a phenomenon is often observed in modeling “simple regimes” of rate-independent models [27, p. 1010] and such is the employed model without the eddy current. The average number of iterations per time level did not depend on the mesh and increased from 3.7 for  $\tau = 5$  s to 4.5 for  $\tau = 50$  s.

Our second example is a hollow ferromagnetic cylinder with the cross section  $r_1 \leq r \leq r_2$ ; such a configuration can be employed for magnetic shielding. If the eddy current is neglected and the magnetic permeability of the material is constant, the problem can be solved analytically [28]. In this case, the magnetic field inside the hole is uniform

$$\mathbf{h} = \frac{4\mu_r \mathbf{h}_e}{(\mu_r + 1)^2 - (r_1/r_2)^2(\mu_r - 1)^2}.$$

Assuming the steel resistivity  $\rho = 0.43 \mu\Omega\cdot\text{m}$  [20] and taking  $r_1 = 0.1$  m and  $r_2 = 0.15$  m, we solved the magnetization problem taking both the eddy current and the hysteresis into account. We now triangulated a larger than the cross section domain, the square  $-0.2 \leq x, y \leq 0.2$  m (see Fig. 9). The mesh contains 6424 triangles; 2352 of them belong to the ferromagnetic domain. Although our numerical algorithm needs only the latter elements, to find the magnetic induction also outside the ferromagnet, we computed the elements of matrices (29)–(34) for all triangle pairs  $e, e'$ , where at least one of the triangles belongs to the magnetic domain (the remaining elements of these matrices can be set to zero). We set  $\mathbf{h}_e = (10^3 t, 0)$  A/m for the first 100 s and assumed that in the next 100 s, the external field rotates 90° counterclockwise with a constant angular velocity, its magnitude remaining at  $10^5$  A/m. The time steps  $\tau = 10$  s and  $\tau = 2.5$  s were used, respectively, for these two time intervals; on average, convergence with the relative tolerance  $10^{-6}$  was achieved in five iterations per time level. Numerical simulation results for  $t = 100$  s and  $t = 200$  s are shown in Fig. 10. A further decrease of the time steps does not change these results.

The eddy current density is not negligible now but, according to our computation, for the assumed external field variation rate, the power of the eddy current loss per unit of length,  $p_j = \int_{\Omega} \rho j^2 d\mathbf{r}$ , is smaller than the power of the magnetization dissipation  $p_m = \mu_0 \int_{\Omega} \{\sum_l k^l |\dot{\mathbf{m}}^l|\} d\mathbf{r}$ . Thus, in the

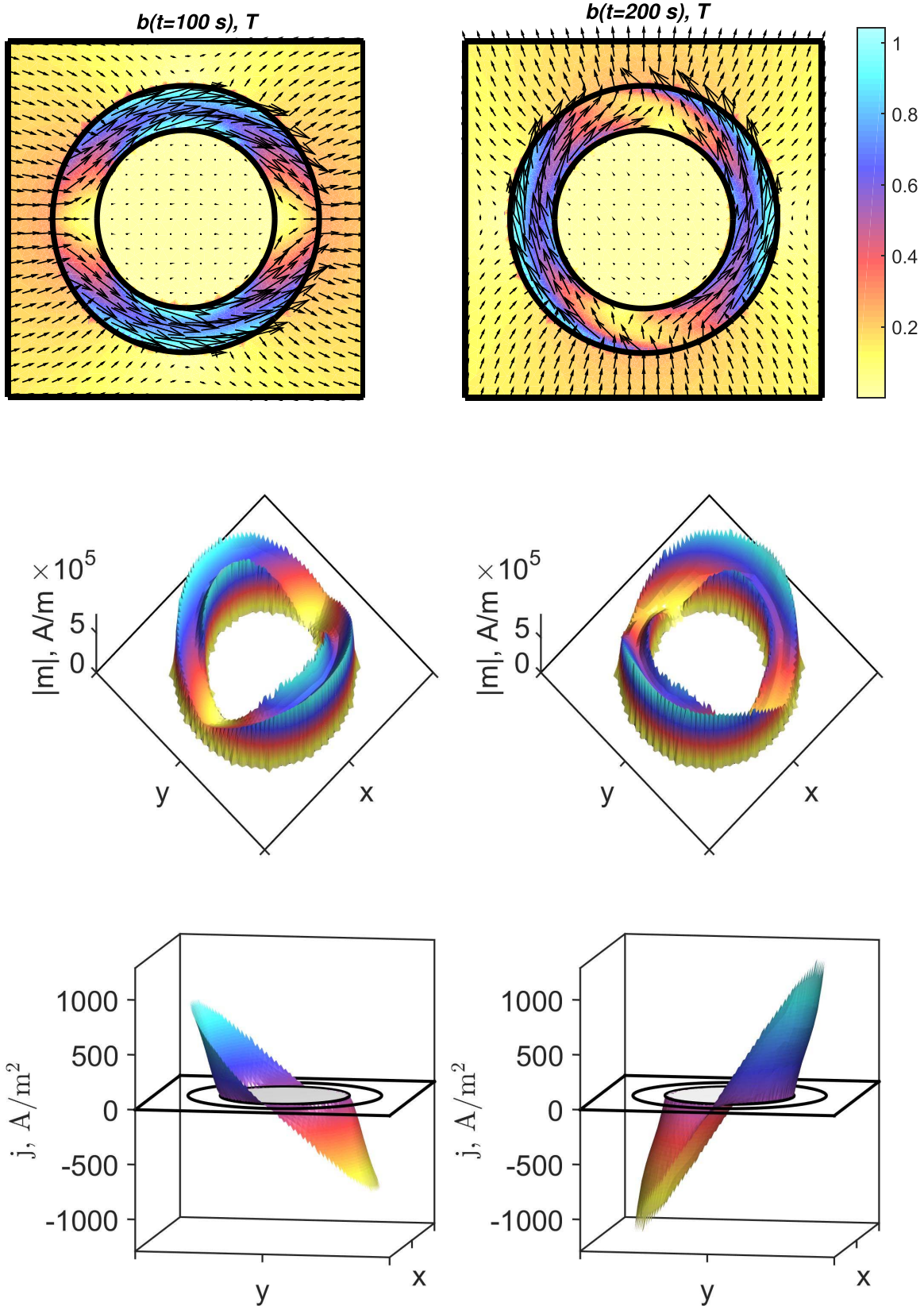


Fig. 10. Numerical simulation. Left: solution for  $t = 100 \text{ s}$ . Right: for  $t = 200 \text{ s}$ . Top: magnetic induction. Middle: magnetization  $|\mathbf{m}|$ . Bottom: eddy current density (in color online).

end of the linear growth of  $h_e$  ( $t = 100 \text{ s}$ ), we obtained  $p_j = 2.4 \cdot 10^{-3} \text{ W/m}$  and  $p_m = 15 \cdot 10^{-3} \text{ W/m}$ ; at  $t = 200 \text{ s}$  (rotating  $\mathbf{h}_e$ ), we obtained  $p_j = 5.0 \cdot 10^{-3} \text{ W/m}$

and  $p_m = 20 \cdot 10^{-3} \text{ W/m}$ . The corresponding losses during the whole time interval  $0 < t < 200 \text{ s}$  are 0.70 and  $2.3 \text{ J/m}$ , respectively. It may be noted that not only the eddy current

density but also the related part of the total loss should increase with the ramping rate of the external field. We also found that the magnetic field inside the cylindrical hole does not exceed 0.14% of  $h_e$  (the shielding effect). Further simulations showed that the pronounced nonmonotonicity of the magnetization  $\mathbf{m}(\mathbf{r}, t)$  in the radial directions [see Fig. 10 (middle)] is caused by the eddy current. Suppressing this current by choosing a high resistivity value makes the solution monotonic radially; qualitatively, for  $t \leq 100$  s, the solution without the eddy current resembles and corresponds to a similar shielding as the analytical solution for an appropriate constant permeability,  $\mu_r \approx 7 \cdot 10^3$ . However, since the magnetic field inside the magnet is not uniform, in the hysteretic (and even simply in the nonlinear) case, obtaining an analytical solution (as we did in the previous example) is not possible. The numerical simulation showed that also the magnetic field inside the hole is not uniform. Finally, we note that, during the rotation of the external field, the magnetization of the inner ring layers lags behind [Fig. 10 (middle-right)], which is the hysteresis effect.

It should be noted that the magnetization model employed here is complicated and cannot compete with much simpler models in terms of the computation time. Even after the matrices (29)–(34) were computed, our MATLAB program still needed several hours to solve examples like these on a standard PC. The main elements, determining the efficiency of our computations are: the integral vector potential formulation, the inner iterations for updating the magnetization of pseudoparticles in each finite element, and the outer iterations for solving (24)–(27) using (28).

Integral formulations like this (we followed [23]) are often employed for solving electrical engineering problems, in general, and eddy current problems, in particular. Their main advantage is that all computations are confined to the area occupied by the conducting and/or magnetic materials; but a disadvantage is the linear systems with dense matrices. Overall, such formulations are competitive with other formulations used for finite-element approximations.

The inner iterations converged in two to three iterations, much faster than in [13], and as was shown above (see Fig. 3), the faster approach based on the explicit approximation (13) can be inexact.

As is well known, for nonlinear materials with high differential susceptibility values, it is difficult to obtain good convergence of iterations in finite-element simulations, especially, if the Newton method cannot be employed. This is the case for the model employed here: in the Newton-like method that we used, the necessary derivatives could only be numerically approximated, and for steel in our simulations, the maximal susceptibility exceeded  $10^5$ . Nevertheless, we were able to reach convergence in five iterations per time level in the outer cycle of our scheme, which is a fast convergence.

## VII. CONCLUSION

Like most existing macroscopic models for ferromagnetic hysteresis, the quasi-static model proposed by Bergqvist [7] is phenomenological. However, it is based upon consistent

energy arguments and a clear albeit simplified physical picture of the dry-friction-like pinning of the domain walls. This model is naturally vectorial, has a variational formulation convenient for numerical simulations, and can be incorporated into a finite-element code as a local constitutive relation with memory. As an example, we considered a problem, where both the magnetization and eddy current were considered.

In this paper, we tried to clarify the mathematical derivation of the variational formulation, extended it to the anisotropic case, proposed an efficient numerical method based on this formulation, and also demonstrated that the usually employed approximation, which turns the model into a play hysteron model, can be inaccurate. We showed that this approximation is not a possible version of the dry-friction law, as is typically assumed, but a replacement by an alternative assumption, not related to dry-friction, and determining a different direction of the system's evolution in the vectorial case.

The model has sufficient degrees of freedom to be fitted to hysteretic behavior of different materials; here, we presented a method for the identification of the parameters in this model using a set of experimental FORCs. Another advantage of this model is its ability to predict both the stored and dissipated energies at any moment in time. These properties make the model highly attractive; its further comparison to experiments would be desirable.

## APPENDIX A NEWTON'S METHOD FOR (12)

Let  $\mathbf{u}(\phi) = \mathbf{h}(t) + k[\cos \phi, \sin \phi]^T$ . Then,  $g(\phi) = S(\mathbf{u}(\phi)) - \check{\mathbf{m}} \cdot \mathbf{u}(\phi)$  and we solve  $g'(\phi) = 0$  iteratively,  $\phi_{n+1} = \phi_n - g'(\phi_n)/g''(\phi_n)$ , with  $\phi_0$  being the direction of  $k^{-1}(\check{\mathbf{h}}_r - \mathbf{h}(t))$ . Here

$$\begin{aligned} g' &= \{\nabla S(\mathbf{u}) - \check{\mathbf{m}}\} \cdot \mathbf{u}' = \left\{ \frac{M(u)}{u} \mathbf{u} - \check{\mathbf{m}} \right\} \cdot \mathbf{u}' \\ g'' &= \left\{ \nabla \left( \frac{M(u)}{u} \right) \cdot \mathbf{u}' \right\} \mathbf{u} \cdot \mathbf{u}' + \frac{M(u)}{u} \mathbf{u}' \cdot \mathbf{u}' \\ &\quad + \left\{ \frac{M(u)}{u} \mathbf{u} - \check{\mathbf{m}} \right\} \cdot \mathbf{u}'' \end{aligned}$$

where  $\mathbf{u}' = k[-\sin \phi, \cos \phi]^T$ ,  $\mathbf{u}'' = -k[\cos \phi, \sin \phi]^T$  and

$$\nabla \left( \frac{M(u)}{u} \right) = \frac{d}{du} \left( \frac{M(u)}{u} \right) \frac{\mathbf{u}}{u} = \frac{u M' - M \mathbf{u}}{u^2}.$$

## APPENDIX B COMPUTATION OF THE INTEGRALS (29)–(34)

To compute the integrals (29)–(34) for any distant pair of triangles  $e, e'$ , we used a symmetric seven point quadrature rule for triangles, exact for all polynomials of degree five [29] (the triangles were regarded as distant if the distance between their centers exceeded several characteristic triangle sizes). For the coinciding, touching, and also close to each other triangles  $e$  and  $e'$ , we employed the representation [32, p. 305]  $G(\mathbf{r}) = \Delta U(\mathbf{r}) - (1/2\pi)$ , where  $U(\mathbf{r}) = -(1/8\pi)r^2 \ln(r)$ ; this yields

$$\begin{aligned} &\int_e \int_{e'} G(\mathbf{r} - \mathbf{r}') d\mathbf{r}' d\mathbf{r} \\ &= \int_e \int_{e'} \Delta U(\mathbf{r} - \mathbf{r}') d\mathbf{r}' d\mathbf{r} - \frac{|e||e'|}{2\pi}. \end{aligned}$$

In addition, we have that

$$\begin{aligned} & \int_e \int_{e'} \Delta U(\mathbf{r} - \mathbf{r}') d\mathbf{r}' d\mathbf{r} \\ &= - \int_e \nabla \cdot \int_{e'} \nabla' U(\mathbf{r} - \mathbf{r}') d\mathbf{r}' d\mathbf{r} \\ &= - \oint_{\partial e} \mathbf{n} \cdot \left\{ \int_{e'} \nabla' U(\mathbf{r} - \mathbf{r}') d\mathbf{r}' \right\} dl \\ &= - \oint_{\partial e} \left\{ \int_{e'} \nabla' \cdot [U(\mathbf{r} - \mathbf{r}') \mathbf{n}] d\mathbf{r}' \right\} dl \\ &= - \oint_{\partial e} \oint_{\partial e'} U(\mathbf{r} - \mathbf{r}') \mathbf{n} \cdot \mathbf{n}' dl' dl \end{aligned}$$

where  $\mathbf{n}$  is the outward unit normal to the boundary  $\partial e$  of  $e$ . Similarly, for example

$$\begin{aligned} & \int_e \int_{e'} \partial_{xx}^2 G(\mathbf{r} - \mathbf{r}') d\mathbf{r}' d\mathbf{r} \\ &= - \oint_{\partial e} \oint_{\partial e'} \partial_{xx}^2 U(\mathbf{r} - \mathbf{r}') \mathbf{n} \cdot \mathbf{n}' dl' dl \end{aligned}$$

so all double surface integrals can be written as a sum of integrals over pairs of edges of the triangles. We note that all such integrals of  $U$  and its first derivatives

$$\partial_x U = -\frac{(\ln(r^2) + 1)x}{8\pi}, \quad \partial_y U = -\frac{(\ln(r^2) + 1)y}{8\pi}$$

are regular. These integrals were computed numerically with a controlled accuracy. The integrals of

$$\begin{aligned} \partial_{xy}^2 U &= -\frac{xy}{4\pi r^2} \\ \partial_{xx}^2 U &= -\frac{1}{8\pi} \left( \frac{2x^2}{r^2} + \ln(r^2) + 1 \right) \\ \partial_{yy}^2 U &= -\frac{1}{8\pi} \left( \frac{2y^2}{r^2} + \ln(r^2) + 1 \right) \end{aligned}$$

were calculated analytically if the two edges coincided or had a common vertex (we used the MATLAB Symbolic toolbox 6.1 in the latter case); otherwise, these integrals are also regular and were computed numerically.

## REFERENCES

- [1] I. D. Mayergoyz, *Mathematical Models of Hysteresis*. New York, NY, USA: Springer, 1991.
- [2] D. C. Jiles and D. L. Atherton, "Theory of ferromagnetic hysteresis," *J. Magn. Magn. Mater.*, vol. 61, nos. 1–2, pp. 48–60, Sep. 1986.
- [3] K. H. Carpenter, "A differential equation approach to minor loops in the Jiles–Atherton hysteresis model," *IEEE Trans. Magn.*, vol. 27, no. 6, pp. 4404–4406, Nov. 1991.
- [4] D. Miljavec and B. Zidarić, "Introducing a domain flexing function in the Jiles–Atherton hysteresis model," *J. Magn. Magn. Mater.*, vol. 320, no. 5, pp. 763–768, 2008.
- [5] S. E. Zirka, I. Y. Moroz, R. G. Harrison, and K. Chwastek, "On physical aspects of the Jiles–Atherton hysteresis models," *J. Appl. Phys.*, vol. 112, no. 4, p. 043916, 2012.
- [6] G. Friedman and I. D. Mayergoyz, "Hysteretic energy losses in media described by vector Preisach model," *IEEE Trans. Magn.*, vol. 34, no. 4, pp. 1270–1272, Jul. 1998.
- [7] A. Bergqvist, "Magnetic vector hysteresis model with dry friction-like pinning," *Phys. B, Condens. Matter*, vol. 233, no. 4, pp. 342–347, 1997.
- [8] A. Bergqvist, A. Lundgren, and G. Engdahl, "Experimental testing of an anisotropic vector hysteresis model," *IEEE Trans. Magn.*, vol. 33, no. 5, pp. 4152–4154, Sep. 1997.
- [9] J. H. Krah and A. J. Bergqvist, "Numerical optimization of a hysteresis model," *Phys. B*, vol. 343, pp. 35–38, Jan. 2004.
- [10] F. Henrotte, A. Nicolet, and K. Hameyer, "An energy-based vector hysteresis model for ferromagnetic materials," *COMPEL-Int. J. Comput. Math. Electr. Electron. Eng.*, vol. 25, no. 1, pp. 71–80, 2006.
- [11] F. Henrotte and K. Hameyer, "A dynamical vector hysteresis model based on an energy approach," *IEEE Trans. Magn.*, vol. 42, no. 4, pp. 899–902, Apr. 2006.
- [12] S. Steentjes, D. Eggers, and K. Hameyer, "Application and verification of a dynamic vector-hysteresis model," *IEEE Trans. Magn.*, vol. 48, no. 11, pp. 3379–3382, Nov. 2012.
- [13] V. François-Lavet, F. Henrotte, L. Stainier, L. Noels, and C. Geuzaine, "An energy-based variational model of ferromagnetic hysteresis for finite element computations," *J. Comput. Appl. Math.*, vol. 246, pp. 243–250, Jul. 2013.
- [14] F. Henrotte, S. Steentjes, K. Hameyer, and C. Geuzaine, "Iron loss calculation in steel laminations at high frequencies," *IEEE Trans. Magn.*, vol. 50, no. 2, Feb. 2014, Art. no. 7008104.
- [15] D. Lin, P. Zhou, and A. Bergqvist, "Improved vector play model and parameter identification for magnetic hysteresis materials," *IEEE Trans. Magn.*, vol. 50, no. 2, Feb. 2014, Art. no. 7008704.
- [16] J. J. Moreau, "Application of convex analysis to the treatment of elastoplastic systems," in *Applications of Methods of Functional Analysis to Problems in Mechanics* (Lecture Notes in Mathematics), vol. 503, P. Germain and B. Nayroles, Eds. Berlin, Germany: Springer-Verlag, 1976, pp. 56–89.
- [17] E. D. Torre, *Magnetic Hysteresis*. Piscataway, NJ, USA: IEEE Press, 1999.
- [18] C. Appino, C. Ragusa, and F. Fiorillo, "Can rotational magnetization be theoretically assessed?" *Int. J. Appl. Electromagn. Mech.*, vol. 44, nos. 3–4, pp. 355–370, 2014.
- [19] D. Lin, P. Zhou, and N. Chen, "A new vector hysteresis model based on series-distributed play hysterons," in *Proc. COMPUFAG*, Montreal, QC, Canada, 2015.
- [20] S. E. Zirka, Y. I. Moroz, P. Marketos, and A. J. Moses, "Viscosity-based magnetodynamic model of soft magnetic materials," *IEEE Trans. Magn.*, vol. 42, no. 9, pp. 2121–2132, Sep. 2006.
- [21] S. E. Zirka, Y. I. Moroz, and R. G. Harrison, "Inverse hysteresis models for transient simulation," *IEEE Trans. Power Del.*, vol. 29, no. 2, pp. 552–559, Apr. 2014.
- [22] F. Liorzou, B. Phelps, and D. L. Atherton, "Macroscopic models of magnetization," *IEEE Trans. Magn.*, vol. 36, no. 2, pp. 418–428, Mar. 2000.
- [23] M. d'Aquino, G. Rubinacci, A. Tamburino, and S. Ventre, "Efficient numerical solution of magnetic field problems in presence of hysteretic media for nondestructive evaluation," *IEEE Trans. Magn.*, vol. 49, no. 7, pp. 3167–3170, Jul. 2013.
- [24] S. E. Zirka, Y. I. Moroz, P. Marketos, and A. J. Moses, "Loss separation in nonoriented electrical steels," *IEEE Trans. Magn.*, vol. 46, no. 2, pp. 286–289, Sep. 2010.
- [25] L. Prigozhin, "Analysis of critical-state problems in type-II superconductivity," *IEEE Trans. Appl. Supercond.*, vol. 7, no. 4, pp. 3866–3873, Dec. 1997.
- [26] J. D. Jackson, *Classical Electrodynamics*. New York, NY, USA: Wiley, 1988.
- [27] J. W. Barrett and L. Prigozhin, "Existence and approximation of a mixed formulation for thin film magnetization problems in superconductivity," *Math. Models Methods Appl. Sci.*, vol. 24, no. 5, pp. 991–1015, 2014.
- [28] L. A. Bessonov, *Theoretical Foundations of Electrical Engineering. Electromagnetic Field*, (in Russian). Moscow, Russia: Uraite, 2016.
- [29] J. Burkhardt, *STRANG7 Quadrature for Triangles*, accessed on Aug. 19, 2016. [Online]. Available: [https://people.sc.fsu.edu/~jburrhardt/datasets/quadrature\\_rules\\_tri/quadrature\\_rules\\_tri.html](https://people.sc.fsu.edu/~jburrhardt/datasets/quadrature_rules_tri/quadrature_rules_tri.html)
- [30] J. T. Katsikadelis, *Boundary Elements: Theory and Applications*. Amsterdam, The Netherlands: Elsevier, 2002.